# Dihydropteroate synthase from Streptococcus pneumoniae: structure, ligand recognition and mechanism of sulfonamide resistance

Colin Levy, David Minnis, Jeremy P Derrick

# DIHYDROPTEROATE SYNTHASE FROM *Streptococcus pneumoniae:* STRUCTURE, LIGAND RECOGNITION AND MECHANISM OF SULFONAMIDE RESISTANCE

**Colin Levy, David Minnis and Jeremy P. Derrick***

**Manchester Interdisciplinary Biocentre and Faculty of Life Sciences, The University of Manchester, Manchester, U.K.**

*Corresponding author: Jeremy.Derrick@manchester.ac.uk

Short title: Dihydropteroate synthase from *S. pneumoniae*

Word count: 5,636

Dihydropteroate synthase (DHPS) catalyses an essential step in the biosynthesis of folic acid and is the target for the sulfonamide group of antimicrobial drugs. Here we report two crystal structures of DHPS from the respiratory pathogen *Streptococcus pneumoniae:* the apoenzyme at 1.8-Å resolution and a complex with 6-hydroxymethyl-7,8-dihydropterin monophosphate at 2.4-Å resolution. The enzyme forms a $\alpha/\beta$ barrel structure, with a highly conserved binding pocket for recognition of the pterin substrate, 6-hydroxymethyl-7,8-dihydropterin pyrophosphate (DHPPP). There is a fixed order of substrate binding: DHPPP binds first, followed by the second substrate, *para*-aminobenzoic acid (pABA). Binding of pyrophosphate also allows the enzyme to recognise pABA or sulfonamide drugs, which act as pABA analogues. Using equilibrium and pre-steady state kinetic fluorescence measurements, we show that the on-rate for DHPPP binding to the enzyme is relatively slow ($2.6 \times 10^5$ $M^{-1}s^{-1}$) and propose that binding of this substrate induces a large scale movement of the second loop in the enzyme structure, to participate in formation of the pABA binding site. Two mutations, which confer resistance to sulfonamide drugs, do not affect DHPPP binding but have a substantial effect on pABA and sulfonamide recognition. The results show that binding of DHPPP and pABA are separate, distinguishable events in the reaction cycle, and that mutations which confer resistance to sulfonamide drugs act exclusively on the second step in the binding process.

Folic acid is an essential component of the diet for higher organisms, including humans. Bacteria, plants and some disease-causing parasites have the ability to synthesize folic acid *de novo*: a sequence of six chemical steps transforms GTP into dihydrofolate (reviewed in [1]). Several enzymes from the folate pathway have no equivalent in man, making them ideal candidates as targets for antimicrobial drugs. Consequently, there has been continuing interest in the structures and mechanisms of the folate biosynthesis enzymes [2-6]. Dihydropteroate synthase (DHPS[1]; EC 2.5.1.15) catalyses an essential step within the folic acid biosynthetic pathway: nucleophilic attack by the amino group of *para*-aminobenzoic acid (pABA) displaces pyrophosphate (PPi) from dihydrohydroxymethylpterin pyrophosphate (DHPPP), leading to the formation of dihydropteroate (Fig 1). This chemical step constitutes a pivotal point in the folate pathway: pABA is synthesized by the chorismate pathway [7] and feeds into the folic acid biosynthesis pathway at this point. The sulfonamides, which were essentially the first group of synthetic antibiotics to be widely used, are potent inhibitors of DHPS [8]. They inhibit the reaction by acting as alternative substrates [9], leading to a 'dead end' sulfa-pterin product. Resistance to sulfonamides is widespread in bacteria and parasites, and generally correlates with mutations to the *dhps* gene [10]. Steady state kinetic analysis has shown that sulfonamide resistance mutations lead to raised $K_i$ values for the drug [10-12].

The crystal structures of DHPS have been determined from a variety of bacterial sources: *E. coli* [13], *S. aureus* [14], *M. tuberculosis* [15] and *B.anthracis* [16]. In addition, the structure of a bifunctional complex of DHPS fused to the preceding enzyme in the pathway, HPPK, has been reported from *S. cerevisiae* [4]. DHPS adopts a α/β (TIM) barrel fold, with the active site identified at one end of the barrel by cocrystallization with a variety of pterin ligands [1]. The DHPS enzymes are structurally related to methyltetrahydrofolate-dependent methyltransferase, and conservation of the pterin binding sites between the two enzymes has been noted [17]. Complexes of several DHPS enzymes bound to the oxidised form of the substrate, 6-hydroxymethylpterin pyrophosphate, or 6-hydroxymethylpterin phosphate, which presumably acts as an inhibitor of the enzyme, show the same orientation of the bound pterin ring [4, 14-16]. Comparisons between different DHPS structures do show, however, that there are significant variations in the conformations of some of the loop regions in the vicinity of the active site. Loop regions 1 and 2, which are likely to be of importance to catalysis, show a variety of conformations or else are absent from electron density maps, suggesting a high degree of conformational flexibility. This has complicated the identification of the binding site for the second substrate, pABA. Achari *et al.* [13] reported the structure of a ternary complex of *E.coli* DHPS with dihydropterin and sulfanilamide, a sulfonamide which acts as an analogue of pABA. Although *E.coli* DHPS is able to use sulfonamides as substrates [9], this structure did not allow an unambiguous reconstruction of the transition state within the active site, as the amino group within sulfanilamide was not aligned for optimal $S_N2$ attack of the DHPPP substrate. An alternative orientation of the pABA aromatic ring was suggested from a more recent report of the cocrystallization of *B.anthracis* DHPS with pteroic acid, an analogue of dihydropteroate [16]. These authors proposed a different location for the pABA binding site, with an orientation more suited to the $S_N2$ attack of the methylene carbon attached to the C6 position on the DHPPP pterin ring. To date, a crystal structure of DHPS with pABA bound has not been fully described and the precise location of the second substrate during the reaction cycle remains an open question.

*Streptococcus pneumoniae* is a respiratory pathogen and a major cause of community-acquired pneumonia; resistance of streptococcal clinical isolates to antibiotics is now common [18]. Sequencing of the *dhps* gene from *S. pneumoniae* has shown that one or two residue insertions, within the predicted loop 2 of the enzyme, are responsible for sulfonamide resistance [19, 20]. A more general survey of the distribution of sulfonamide resistance mutations established that they tended to cluster to sites within loops 1 and 2 [15]. Interestingly, alignments of *dhps* gene sequences show regions of relatively high sequence

[1] The abbrevations used are: DHPS, dihydropteroate synthase; DHPPP, 6-hydroxylmethyl-7,8-dihydropterin pyrophosphate; DHPP, 6-hydroxylmethyl-7,8-dihydropterin monophosphate; pABA, *para*-aminobenzoic acid; PPi, pyrophosphate.

conservation within these same regions [15, 16], suggesting that they may be involved in pABA recognition. Although sulfonamides are no longer in extensive clinical use, there are compelling reasons to try to understand the origin of sulfonamide resistance. First, DHPS is one of the few biosynthetic enzymes which have been successfully exploited as targets for antimicrobial drugs. Knowledge of the structure and mechanism of the enzyme could be employed to develop a more informed approach to drug design, perhaps by exploitation of the conserved DHPPP binding site [16, 21]. Second, the structural similarity between sulfonamides and pABA raises an intruiging question: how can a single site mutation permit DHPS to discriminate between them? To date, relatively few enzymological studies on DHPS have been reported, and are mainly confined to steady state kinetics [10, 11, 22]. Here, we have exploited fluorescence-based equilibrium and pre-steady state kinetic binding studies, in combination with crystallography, to examine the structural changes which occur in DHPS on binding substrates. *S. pneumoniae* DHPS is an ideal enzyme for this work, as it lends itself to binding measurements using the intrinsic fluorescence of the protein, as well as the fluorescence of DHPPP. The results suggest that extensive structural changes occur within the second loop region on binding the first substrate (DHPPP) and that sulfonamide resistance mutations in this loop have a drastic effect on pABA binding.

## Experimental

*Materials.* 6-hydroxymethyl pterin pyrophosphate was obtained from Schirks Laboratories and reduced using sodium dithionite to DHPPP as described previously [23]. Selenomethionine, pABA and sulfamethoxazole were obtained from Sigma.

*Protein Expression and Purification.* The cloning and expression in *E. coli* of DHPS from *S. pneumoniae* has been described previously [22]. A similar method was employed to that described by Vinnicombe and Derrick for purification of the enzyme from *E. coli*, with some modifications. Competent XL2 blue *E.coli* cells (Stratagene, La Jolla, CA) were transformed with the expression plasmid and grown in LB broth [24], supplemented with 100 μg/ml ampicillin at 37°C. Expression of DHPS was induced by addition of isopropyl-β-D-thiogalactopyranoside (IPTG) at a final concentration of 1 mM; cells were allowed to grow for a further 3 hours after induction before being harvested by centrifugation for 20 min at 5,000$g_{av}$. For production of DHPS with selenomethionine incorporation, growth was conducted in a defined medium designed to suppress methionine biosynthesis [25]. The cell pellet was washed twice with 10 ml of lysis buffer (100 mM Tris-HCl pH 8.0, 50 mM NaCl, 1 Complete protease inhibitor tablet/50 ml (Roche, Basel, Switzerland)), 1 mM DTT, 1 mM EDTA and then resuspended in 50 ml of lysis buffer. Cells were lysed by sonication, and the cell debris was sedimented by centrifugation at 20,000$g_{av}$ for 30 min at 4°C. The supernatant was retained, ammonium sulfate added to 50% saturation and the solution left on ice for 1 hour. The resulting precipitate, containing DHPS, was retrieved by centrifugation at 20,000$g_{av}$ for 15 min at 4°C. The precipitate was resuspended in 50 ml re-suspension buffer (20 mM Tris-HCl pH 8.0) and dialysed overnight against 5 L of the same buffer. The enzyme was then subjected to ion exchange chromatography using a Resource Q column (GE. Healthcare Bio-Sciences Corp. Uppsala, Sweden), equilibrated in 20 mM Tris-HCl (pH 8.0). DHPS was eluted by application of a linear gradient from 0 to 1 M NaCl in the same buffer; appropriate fractions were identified by SDS-PAGE, pooled and dialysed overnight against re-suspension buffer. The protein preparation was then subjected to a second ion exchange step, using a Mono Q column (GE. Healthcare Bio-Sciences Corp. Uppsala, Sweden), equilibrated in 20 mM Tris-HCl (pH 8.0). DHPS was eluted by application of a linear gradient from 0 to 1M NaCl in the same buffer. At this stage the DHPS preparation was sufficiently pure for use in kinetics or binding studies. However, for crystallization a final purification step was found to assist in crystal growth. The appropriate fractions from the Mono Q column were pooled, concentrated to a final volume of 2.0 ml and applied to a Superdex 200 gel filtration column (GE. Healthcare Bio-Sciences Corp. Uppsala, Sweden), equilibrated in 20 mM Tris-HCl (pH 8.0), 150 mM NaCl. The enzyme eluted in a single peak: the appropriate fractions were pooled and dialysed overnight against 20 mM Tris-HCl (pH 8.0).

*Site-directed mutagenesis*. Site-specific mutations were introduced by using the Quikchange mutagenesis kit (Stratagene) and following manufacturer's instructions.

*Crystallization and Data Collection***.** Purified DHPS was concentrated by ultrafiltration to a protein concentration of 13 mg/ml. Rod-shaped crystals were grown by the hanging drop method, by mixing 2 µl of the protein solution with 2 µl of the well solution, consisting of 0.2 M ammonium iodide and 20% (w/v) polyethylene glycol 3,350. The crystals generally appeared within 7-14 days. Crystals of selenomethionine-incorporated DHPS were grown in the same way. To obtain the complex with 6-hydroxymethyl-7,8-dihydropterin monophosphate (DHPP), hanging drop crystallization trials were set up as described for native and selenomethione DHPS, but with the inclusion of 2.5 mM 6-hydroxymethyl-7,8-dihydropterin pyrophosphate (DHPPP) and 10 mM $MgCl_2$ in the drop. In the case of the DHPP complex, crystals were grown in an anaerobic chamber (Belle, U.K.) which maintained the oxygen level at less than 1.0 ppm and prevented oxidation of the ligand. For data collection, crystals were briefly immersed in Paratone-N, removed using a cryoloop (Hampton Research) and frozen rapidly in liquid nitrogen. For crystals grown under low oxygen conditions, freezing was carried out within the anaerobic chamber. All crystals were maintained at 100K by a stream of dry nitrogen during data collection. Data collection statistics are given in Table 1. Laboratory data for the DHPP complex were collected on a Rigaku MicroMax007 rotating anode X-ray generator and R-AXIS IV++ image plate detector. All data were processed using d*TREK, as implemented in CrystalClear [26].

*Structure Determination and Refinement.* Attempts to solve the structure of *S. pneumoniae* DHPS from the native 1.8-Å resolution dataset by molecular replacement, using DHPS structures from *E.coli*, *S.aureus, M.tuberculosis* and *B.anthracis,* gave ambiguous results. *S. pneumoniae* DHPS was therefore prepared with selenomethionine incorporation: crystals from this preparation formed a different spacegroup from the native dataset (Table 1). A dataset was collected at a single wavelength, and subjected to single-wavelength anomalous diffraction (SAD) phasing and automated model building using the SOLVE/RESOLVE package [27]. The resulting partial model was taken as the input for molecular replacement of the native 1.8-Å resolution dataset using PHASER [28]. Iterative rounds of rebuilding and maximum likelihood refinement were carried out using COOT [29] and the CCP4 program REFMAC5 [30], as implemented within the CCP4 suite [31]. The structure comprised a dimer in the asymmetric unit, and no non-crystallographic symmetry restraints were applied during refinement. The final structure was missing residues 1-6 (chain A), 1-5 (chain B) from the N-terminus, and residues 304-314 (chain A) and 303-314 (chain B) from the C-terminus. In addition, electron density was either weak or absent, and therefore also omitted from the final structure, from the following residue ranges: 21-29 (chain A), 20-31 (chain B), 57-61 (chain A), 57-62 (chain B), 157-158 (chain A) and 156-159 (chain B). Stereochemical parameters, determined using PROCHECK [32], were within the expected ranges, or better, for a structure determined at 1.8-Å resolution. Refinement statistics are summarized in Table 1. The native structure was used to solve the structure of the complex with DHPP bound which was the same crystal form. Again, refinement was carried out using REFMAC5 [30]. The Protein Data Bank Accession codes are 2VEF and 2VEG for the apoenzyme and DHPP complexes respectively.

*Fluorimetric titration assays.* Equilibrium fluorescence titrations were recorded using a Varian Cary Eclipse fluorescence spectrophotometer. To determine the equilibrium binding constant ($K_d$) for PPi binding to the sulfonamide sensitive form of DHPS, an excitation wavelength of 290 nm (2.5 nm slit) and an emission wavelength of 340 nm (10 nm slit) were employed. Titration was carried out in a fluorescence cuvette with a volume of 3 ml, containing 50 mM Tris-HCl (pH 8.0), 5 mM $MgCl_2$ (the same buffer as employed by Vinnicombe and Derrick[22]) and a protein concentration of 50 µg/ml. For determination of the binding of pABA to the sulfonamide sensitive form of DHPS, an excitation wavelength of 265 nm (2.5 nm slit) and an emission wavelength of 340 nm (10 nm slit) were employed. Typically, four separate readings were averaged at each point in the titration. The pABA titration required correction for the inner filter effect arising from pABA absorption: data from a control titration, with no enzyme, was used to establish the correction parameters as described by Birdsall *et al.* [33]. Determination of the $K_d$ for binding of pABA to the Y63 and GS60 sulfonamide resistance mutants required a different approach, as their binding affinity for pABA was reduced. Titrations of PPi into a solution of 150 µg/ml DHPS in Tris/$MgCl_2$ buffer was carried out, in the presence of varying concentrations of pABA. Fluorimeter settings, excitation and emission wavelengths were the same as those used for the titration of PPi into the

sulfonamide sensitive form of DHPS. All fluorescence equilibrium binding data were fitted to the binding models given in the text using the software package DYNAFIT [34].

*Stopped flow transient kinetics.* Stopped flow fluorescence measurements were carried out using an SX.18MV spectrometer (Applied Photophysics, Leatherhead U.K.). For measurement of the binding of PPi, using the intrinsic tryptophan fluorescence of the enzyme, an excitation wavelength of 290 nm was used, and an emission wavelength of 340 nm, through the use of a second monochrometer. For measurement of pterin fluorescence, an excitation wavelength of 330 nm was used, in combination with a cutoff filter of 400nm in line with the emission photomultiplier. The temperature of the observation chamber and drive syringes was maintained by water circulation at 25°C. The mixing ratio was 1:1 for all experiments. Solutions of ligands and enzyme were prepared by dilution into 50 mM TrisHCl (pH 8.0), 5 mM $MgCl_2$: precautions to maintain an anaerobic environment were implemented as described previously [23]. Data acquisition and processing were controlled by a 32-bit RISC processor workstation.

**Results**

In order to investigate the mechanism of substrate binding and sulfonamide resistance in *S. pneumoniae* DHPS, it was valuable to determine the crystal structure of the enzyme. The structure of the *S. pneumoniae* DHPS apoenzyme was refined to 1.8-Å resolution and used to solve the structure of a complex obtained from a DHPS crystal grown in the presence of the pterin-containing substrate DHPPP, to a resolution of 2.4-Å (Table 1). Density for the ligand was observed in only one of the two potential binding sites within the enzyme dimer (Fig 2A & B): a similar phenomenon has been observed in the DHPS structure from *S.aureus* [14]. Furthermore, although density was well defined for the pterin ring and α-phosphate, there was no evidence for presence of the β-phosphate (Fig 2B). Our interpretation of this observation is that the β-phosphate has probably been removed by hydrolysis from the DHPPP ligand during crystallization. For this reason, we will refer to this structure as a complex with 6-hydroxymethyl-7,8-dihydropterin monophosphate (DHPP) i.e. the monophosphorylated form of DHPPP. Determination of the structure of the DHPS:DHPP binary complex enabled identification of the pterin binding site within the enzyme and placed some constraints on the likely location of the PPi moiety in the DHPS:DHPPP structure.

Although there was a dimer in the asymmetric unit, the structures of the two subunits in the apoenzyme structure were essentially identical, with an r.m.s. deviation of 0.73 Å for Cα atoms. This was also the case for the DHPP complex, where the equivalent figure was 0.51 Å. Perhaps surprisingly, there was also little difference between the apoenzyme structure and the DHPP complex (r.m.s. 0.27 Å). The pterin ring of DHPP binds within a well defined cavity on the enzyme surface, with the phosphate group pointing outwards. A mixture of polar and apolar residues line the cavity: Asp91, Asn110, Asp201 and Lys237 form hydrogen bonds to the pterin ring (Fig 2C). Asn17, Arg282 and His284 are involved in recognition of the phosphate moiety within DHPP. These residues are highly conserved in other bacterial enzymes, and have similar functions in pterin and phosphate recognition [13-16]. There was little change in the conformations of the side chains of these residues on binding of DHPP, and no evidence for occupancy of the pterin binding site by a residue from loop 2, as is the case for *B.anthracis* DHPS [16].

*S. pneumoniae* DHPS adopts a TIM barrel-type fold, in common with the structures of DHPS enzymes which have been determined from other sources [4, 13-16]. Even after successive rounds of model building and refinement, electron density for some parts of the polypeptide chains in the native and DHPP complex structures was either weak or absent. In particular loops 1 and 2, which contain a number of highly conserved residues and are the sites for sulfonamide resistance mutations, were poorly defined (Fig 3A). This observation indicates that these loops are highly mobile and that their mobility may be linked to catalysis. The principal core secondary structure elements that define the TIM barrel overlay well with those from other structures, but significant deviations were observed in some loop regions. An example of this variation is presented in Fig 3B, which shows an overlay of DHPS structures from *S. pneumoniae* and *S. aureus*. The L5 loop incorporates three short α-helices in the *S. pneumoniae* structure, but is much shorter in the *S. aureus* enzyme. Other minor differences were also apparent: the loop from the end of the αloop7b helix to α7 is also longer in *S. pneumoniae* DHPS and adopts a different conformation from other bacterial DHPS structures. This modification could be associated with dimer formation, as some residues within this loop region (eg Phe249) form direct contacts with residues in the adjacent subunit.

Numerous attempts were made to obtain structures of *S. pneumoniae* DHPS in complex with PPi, pABA or several sulfonamide drugs, by co-crystallization or ligand soaking. Where crystallographic data were collected and analysed, the resulting structures did not result in any plausible density being obtained for the ligands, although it was noted that soaking with PPi and pABA or sulfonamide led to cracking of the crystals. These observations are consistent with the conclusion that recognition of pABA or sulfonamide requires a specific conformational change from the apoenzyme structure. We therefore sought to examine alternative ways in which pABA and sulfonamide binding could be studied. It has been shown previously, through use of a radiochemical binding assay, that the *S. pneumoniae* DHPS apoenzyme has a very low affinity for pABA or sulfonamides [22]. The binding of PPi to the enzyme dramatically increases the affinity of the enzyme for pABA, presumably because PPi is capable of imitating the substrate DHPPP. An analysis of the binding of PPi to the enzyme will therefore provide some clues to the structural changes which occur on forming the pABA binding site.

*S. pneumoniae* DHPS contains a single tryptophan residue, Trp93: a change in the environment of the side chain of this residue on ligand binding could be reflected in a change in the intrinsic fluorescence of the enzyme. The results of an equilibrium titration of PPi into the enzyme are shown in Fig 4: binding of the ligand produces a 65% enhancement in fluorescence intensity (Fig 4). Data fitting showed that the response was consistent with a single, saturable binding site and gave a $K_d$ of 350±20 μM for the sulfonamide sensitive form of the enzyme. Trp93 is situated in a short loop between the third β-strand and α-helix in the TIM barrel fold, and lies approximately 15 Å from the α-phosphate in the DHPP ligand (Fig 2D). Solvent accessibility calculations, using the method of Lee and Richards [35] and implemented using AREAIMOL from the CCP4 suite [31], established an average area of 28 Å$^2$ for Trp93 across both chains in the apoenzyme dimer. A structural rearrangement on binding of PPi could lead to the indole ring becoming more buried in the DHPS:PPi binary complex, and hence explain the fluorescence enhancement.

It has been established that sulfonamide resistance in *S. pneumoniae* DHPS can be caused by mutations to residues which lie within the second loop region [19, 20]. To examine the effects of sulfonamide resistance mutations on the ligand binding behavior of the enzyme, two resistance mutations were introduced into the coding sequence for the sulfonamide sensitive form of DHPS, and the mutant enzymes expressed and purified. Mutations known to cause sulfonamide resistance frequently involve insertion of one or more residues into the loop regions of the enzyme. We selected two which have previously been shown to confer sulfonamide resistance on *S. pneumoniae* DHPS [19]: Y63 (which denotes insertion of a Tyr residue at position 63) and GS60 (similarly, insertion of a GS dipeptide at position 60). The effect of PPi binding to both these sulfonamide resistant enzymes on the fluorescence of Trp93 was studied (Fig 4). Although the fluorescence yield of each mutant was comparable to the sulfonamide sensitive form of the enzyme, titration of PPi up to a concentration of 2 mM had only a minimal effect on the intrinsic fluorescence- a quench of less than 3%. This value was too small to accurately measure a $K_d$ value for PPi binding. This observation suggested that either the Y63 and GS60 mutations had substantially reduced affinity for PPi, or they had indirectly affected the response of Trp93.

To extract the rate constant for the binding of PPi to the sulfonamide sensitive form of DHPS, the change in intrinsic fluorescence after rapid mixing of enzyme and PPi was recorded by stopped flow. The results showed a rapid rise in fluorescence on binding of PPi over about 100 ms, which could be fitted to a single exponential curve (Fig 5A). The apparent rate constant, $k_{app}$, was recorded over a range of concentrations of PPi, and $k_{on}$ and $k_{off}$ for the binding were deduced as 5.6±0.3 x 10$^4$ M$^{-1}$s$^{-1}$ and 21±1 s$^{-1}$ respectively (Fig 5B). It is interesting to note that the on-rate for PPi binding to the enzyme is relatively slow. It is not possible, from these data, to distinguish between a slow rate of association between PPi and the enzyme, or a rapid binding, followed by a slow isomerization step. The calculated equilibrium $K_d$ ($k_{off}/k_{on}$) is 375 μM, which agrees well with the value obtained by equilibrium fluorescence titration in Fig 4.

Changes in the fluorescence of the pterin ring have been used to measure binding of 6-hydroxymethyl-7,8-dihydropterin to the preceding enzyme in the folate pathway, 6-hydroxymethyl-7,8-dihydropterin pyrophosphokinase [6, 23, 36]. We used a similar approach to measure the binding of the substrate

DHPPP to *S. pneumoniae* DHPS: rapid mixing of the enzyme with DHPPP produced a quench in pterin fluorescence which could be fitted to a single exponential decay (Fig 6A). The on- and off-rates for binding of DHPPP were then determined in an analogous fashion to that employed for the binding of PPi (Fig 6B). $k_{on}$, the on-rate for binding of DHPPP to the enzyme, is about 5 times faster, at 2.6±0.2 x $10^5$ $M^{-1}s^{-1}$, than for PPi binding. As was the case for the PPi binding data shown in Fig 5, it was not possible to determine whether the change in DHPPP fluorescence occurs immediately upon DHPPP binding to the enzyme, or afterwards in a slow isomerization step.

The experiment was repeated for the Y63 and GS60 sulphonamide resistant variants, and the results are summarized in Table 2. It is noteworthy that the calculated equilibrium binding constant for DHPPP is only about one order of magnitude higher, at 33 μM, than that for PPi (350 μM). In thermodynamic terms, this means that addition of the pterin moiety to the PPi ligand only contributes around 6 kJ/mol to the free energy for binding. This is a surprising observation, given that the pterin binding pocket is apparently well adapted to recognition of the pterin ring. It is also clear that the sulfonamide resistance mutations have little effect on the binding of DHPPP, suggesting that both sulfonamide resistant mutants are also capable of binding to PPi with the same affinity as the wild type enzyme. The fluorescence from DHPPP in the enzyme:DHPPP binary complex was similar for the sulfonamide-sensitive and resistant forms of the enzyme. The failure to observe any change in intrinsic enzyme fluorescence on binding of PPi, noted above, is therefore more likely to be due to a difference in the environment of Trp93 in the Y63 and GS60 mutants in the PPi-bound state. Interestingly, determination of the crystal structure of the GS60 mutant apoenzyme, in the same crystal form as the sulfonamide sensitive enzyme form, revealed no significant differences between the two structures (data not presented). Repetition of the stopped flow experiment shown in Fig 6 using DHPP- the ligand identified in the crystal structure- showed no appreciable change in pterin fluorescence on rapid mixing with either the sulfonamide sensitive or resistant forms of the enzyme (data not shown). These observations lead us to conclude that it is primarily the binding of the PPi moiety within the DHPPP substrate which induces a wide-scale rearrangement of the DHPS active site.

We have shown previously that there is no measurable affinity for pABA binding to the *S. pneumoniae* DHPS apoenzyme and suggested that the enzyme (E) adopts a compulsory substrate binding order, with DHPPP binding first, followed by pABA [22]:

$$E \leftrightarrow E{:}DHPPP \leftrightarrow E{:}DHPPP{:}pABA$$

It was also shown that pABA and sulphonamide drugs bind to the E:PPi binary complex [22]. These observations suggest that binding of DHPPP or PPi induces a structural change which forms the pABA binding site. With this binding model in mind, we set out to use a fluorescence method to measure pABA binding to DHPS. The results of a titration of pABA into a solution of the sulfonamide sensitive form of *S. pneumoniae* DHPS and PPi are shown in Fig 7A. pABA is weakly fluorescent, with excitation and emission wavelength maxima of 265 nm and 340 nm respectively. In the absence of enzyme, titration with pABA produces a linear response in fluorescence. In the presence of enzyme, a quench phase in the titration profile is observed (Fig 7A). The data were fitted to a compulsory order binding model, where pABA is only capable of binding to the DHPS:PPi binary complex:

$$E \leftrightarrow E{:}PPi \leftrightarrow E{:}PPi{:}pABA$$

Binding of PPi to DHPS produces an enhancement in fluorescence, as expected from the response of intrinsic DHPS fluorescence to PPi binding shown in Fig 4. The results of the data fitting established that the fluorescence of the E:PPi:pABA ternary complex was substantially quenched relative to the binary complex. The $K_d$ for pABA was determined to be 0.13±0.02 μM. If the fluorescence of DHPS is arbitrarily set at 100%, the relative fluorescence of the binary complex is 173% and the ternary complex (with pABA bound) is 96%. Stopped flow experiments, in which pABA was rapidly mixed with the DHPS:PPi binary complex, indicated that pABA addition was too fast to be measured reliably (less than 10ms; data not shown).

A repetition of the experiment shown in Fig 7A with the Y63 and GS60 sulfonamide resistance mutants showed a much reduced response with increasing pABA concentration, suggesting that the pABA binding affinity of these enzymes was weaker than the sulfonamide-sensitive form (not shown). It was not possible to determine an accurate $K_d$ for pABA binding to the sulfonamide resistance mutants using this approach, so an alternative method was devised: PPi was titrated into a solution containing pABA and DHPS, and the change in fluorescence monitored (Fig 7B). In the case of the sulfonamide resistant enzymes, binding of PPi had little effect on the intrinsic fluorescence (Fig 4): hence the decrease in fluorescence in this experiment is attributable to pABA binding. The experiment was carried out at different concentrations of pABA, and the data were fitted to the same compulsory order binding model given above. The fluorescence of the ternary complex was 10-20% of that for the apoenzyme and DHPS:PPi binary complexes. The $K_d$ for pABA binding to the Y63 variant was determined to 50±6 μM (Fig 7B). Repetition of the same experiment with the GS60 mutant gave a $K_d$ of 16±6 μM for pABA binding (not shown). The results show that the $K_d$ for pABA binding to the resistant mutant enzymes is around 2 orders of magnitude higher relative to that for the sulfonamide sensitive form of the enzyme. The experiment shown in Fig 7B was also adapted to measure binding of a sulfonamide drug, sulfamethoxazole, to the sulfonamide sensitive form of DHPS: this gave a $K_d$ of 2.3±0.1 μM (data not shown). By contrast, repeating the same experiment with the Y63 and GS60 sulfonamide resistant enzymes produced no detectable binding response. The impairment in binding affinity of pABA, caused by the Y63 and GS60 mutations, is therefore also reflected in the binding of a sulfonamide drug.

**Discussion**

The work presented here has shown, through a combination of structural and ligand binding studies, that the binding of DHPPP and pABA to DHPS can be considered as two discrete events and that sulfonamide resistance mutations exclusively affect the second pABA binding step. To date, enzymological studies of DHPS have largely been confined to steady state kinetics [10, 11], and the current knowledge of the DHPS catalytic cycle is rudimentary by comparison with the preceding enzyme in the folate pathway, 6-hydroxymethyl 7,8-dihydropterin pyrophosphokinase, for example [3, 6, 23, 36]. Earlier studies on the effects of sulfonamide resistance mutations have shown changes in steady state kinetic parameters in the DHPS from *Neisseria meningitidis* [11]. $K_M$ values, however, consist of a composite of individual rate constants and are dependent on the kinetic model for the enzyme concerned. Changes in $K_M$ which occur as a result of sulfonamide resistance mutations are difficult to interpret in the absence of such a model. There are therefore obvious strengths in an approach which breaks down the reaction pathway into individual binding steps.

The structure of *S. pneumoniae* DHPS, reported here, shows a highly conserved arrangement of the pterin binding site- a pocket which appears well adapted for recognition of the pterin ring. In the light of this observation, the fact that the binding affinity for DHPPP is only about one order of magnitude higher than that for PPi is surprising. We also find that the on-rates for both DHPPP and PPi binding to the enzyme are relatively slow. Given that binding of these ligands is necessary for pABA/sulfonamide recognition, we infer that association of DHPPP or PPi induces a significant structural change in the enzyme, probably involving several loop regions. This would explain the slow associated fluorescence changes which occur on the binding of DHPPP or PPi. The large enhancement in the fluorescence of Trp93 suggests that PPi binding induces a change in the environment of this residue. The Y63 and GS60 mutations, which are situated in loop 2 (L2 in Fig 3A), do not appear to affect DHPPP binding but do alter the enhancement in Trp93 fluorescence by PPi (Fig 4). Tyr63 lies at the N-terminal end of alpha helix 2 at the end of loop 2 and about 23 Å from the α-phosphate of DHPP; a large conformational change would be required to place this residue close to the likely position of DHPPP. Interestingly, Trp93 lies roughly equidistant between Tyr63 and the DHPP ligand, and is partially exposed to solvent. A restructuring of loop 2 on binding of DHPPP or PPi, such that it packs against Trp93 and contributes to a binding site for pABA or sulfonamide, would be consistent with the results presented here. Presumably sulfonamide resistance mutations would disrupt the conformation of loop 2, altering the interaction with Trp93 and changing its fluorescence properties. It is interesting to note that the structurally equivalent residue to Trp93 in *E.coli* DHPS, Ser98, packs against loop 2 in that structure.

We have also shown that the sulfonamide resistance mutations have a drastic effect on pABA binding affinity for the DHPS-PPi binary complex, increasing the $K_d$ by around 100-fold. The simplest explanation for this observation is that the structure of loop 2 in the DHPS:PPi binary complex is altered by the Y63 or GS60 mutations in such a way as to impair pABA or sulfonamide recognition. In our analysis of the effects of sulfonamide resistance mutations on the $K_d$ for pABA binding to DHPS-PPi, we are making the tacit assumption that the same differences would also be reflected in binding to the DHPS-DHPPP complex. We regard this as a reasonable assumption for the following reasons: we have shown previously that differences in $K_d$ values for sulfonamides binding to DHPS-PPi are reflected in $K_i$ values determined from steady state kinetics [22]. In addition, our observations that PPi and DHPPP binding induce pABA/sulfonamide binding and that both ligands bind with similar affinities to the apoenzyme, support this proposition.

Despite its established importance as a drug target, the mechanism of DHPS remains poorly understood. Although crystal structures of the enzyme have been reported from a variety of organisms, it is not always clear how each structure is related to the reaction pathway. Both the crystal structures reported here, of the apoenzyme and DHPP complex, seem to relate to a form of the enzyme at the beginning of the reaction cycle. We were unable to obtain structures of complexes with DHPPP, or ternary complexes with PPi and pABA. Nevertheless, the results provide evidence for a subtle and dynamic response of the loop regions around the DHPPP binding site, perhaps explaining why intermediate states in the reaction cycle are difficult to crystallize. The precise structure of the pABA binding site remains poorly defined in DHPS from any organism. Our results have shown that the origin of an explanation for the molecular basis for sulfonamide resistance probably lies in changes to the behaviour of the loop regions surrounding the active site. Further work will require characterization of these changes in more detail.

**Acknowledgements**

We thank the Wellcome Trust for grant funding to support this work.

**References**

1 Bermingham, A. and Derrick, J. P. (2002) The folic acid biosynthesis pathway in bacteria: evaluation of potential for antibacterial drug discovery. Bioessays. **24**, 637-648

2 Garçon, A., Levy, C. and Derrick, J. P. (2006) Crystal structure of the bifunctional dihydroneopterin aldolase/6-hydroxymethyl-7,8-dihydropterin pyrophosphokinase from *Streptococcus pneumoniae*. J. Mol. Biol. **360**, 644-653

3 Li, Y., Blaszczyk, J., Wu, Y., Shi, G. B., Ji, X. H. and Yan, H. G. (2005) Is the critical role of loop 3 of Escherichia coli 6-hydroxymethyl-7,8-dihydropterin pyrophosphokinase in catalysis due to loop-3 residues arginine-84 and tryptophan-89? Site-directed mutagenesis, biochemical, and crystallographic studies. Biochemistry. **44**, 8590-8599

4 Lawrence, M. C., Iliades, P., Fernley, R. T., Berglez, J., Pilling, P. A. and Macreadie, I. G. (2005) The three-dimensional structure of the bifunctional 6-hydroxymethyl-7,8-dihydropterin pyrophosphokinase/dihydropteroate synthase of *Saccharomyces cerevisiae*. J. Mol. Biol. **348**, 655-670

5 Goulding, C. W., Apostol, M. I., Sawaya, M. R., Phillips, M., Parseghian, A. and Eisenberg, D. (2005) Regulation by oligomerization in a mycobacterial folate biosynthetic enzyme. J. Mol. Biol. **349**, 61-72

6 Garçon, A., Bermingham, A., Lian, L. Y. and Derrick, J. P. (2004) Kinetic and structural characterization of a product complex of 6-hydroxymethyl-7,8-dihydropterin pyrophosphokinase from *Escherichia coli*. Biochem. J. **380**, 867-873

7 Dosselaere, F. and Vanderleyden, J. (2001) A metabolic node in action: chorismate-utilizing enzymes in microorganisms. Crit. Rev. Microbiol. **27**, 75-131

8 Sammes, P. G. (1990) Sulfonamides and sulfones. In Comprehensive medicinal chemistry (Sammes, P. G. and Taylor, J. B., eds.). pp. 255-270, Pergamon Press, Oxford

9 Roland, S., Ferone, R., Harvey, R. J., Styles, V. L. and Morrison, R. W. (1979) The characteristics and significance of sulfonamides as substrates for *Escherichia coli* dihydropteroate synthase. J. Biol. Chem. **254**, 10337-10345.

10 Sköld, O. (2000) Sulfonamide resistance: mechanisms and trends. Drug Resist Update. **3**, 155-160

11 Fermer, C. and Swedberg, G. (1997) Adaptation to sulfonamide resistance in *Neisseria meningitidis* may have required compensatory changes to retain enzyme function: kinetic analysis of dihydropteroate synthases from *N. meningitidis* expressed in a knockout mutant of *Escherichia coli*. J. Bacteriol. **179**, 831-837.

12 Triglia, T., Menting, J. G., Wilson, C. and Cowman, A. F. (1997) Mutations in dihydropteroate synthase are responsible for sulfone and sulfonamide resistance in *Plasmodium falciparum*. Proc. Natl. Acad. Sci. U. S. A. **94**, 13944-13949.

13 Achari, A., Somers, D. O., Champness, J. N., Bryant, P. K., Rosemond, J. and Stammers, D. K. (1997) Crystal structure of the anti-bacterial sulfonamide drug target dihydropteroate synthase. Nat. Struct. Biol. **4**, 490-497

14 Hampele, I. C., D'Arcy, A., Dale, G. E., Kostrewa, D., Nielsen, J., Oefner, C., Page, M. G., Schonfeld, H. J., Stuber, D. and Then, R. L. (1997) Structure and function of the dihydropteroate synthase from *Staphylococcus aureus*. J. Mol. Biol. **268**, 21-30

15 Baca, A. M., Sirawaraporn, R., Turley, S., Sirawaraporn, W. and Hol, W. G. (2000) Crystal structure of *Mycobacterium tuberculosis* 7,8-dihydropteroate synthase in complex with pterin monophosphate: new insight into the enzymatic mechanism and sulfa-drug action. J. Mol. Biol. **302**, 1193-1212

16 Babaoglu, K., Qi, J. J., Lee, R. E. and White, S. W. (2004) Crystal structure of 7,8-dihydropteroate synthase from *Bacillus anthracis*: Mechanism and novel inhibitor design. Structure. **12**, 1705-1717

17 Doukov, T., Seravalli, J., Stezowski, J. J. and Ragsdale, S. V. (2000) Crystal structure of a methyltetrahydrofolate- and corrinoid-dependent methyltransferase. Structure. **8**, 817-830

18 File, T. M. (2006) Clinical implications and treatment of multiresistant *Streptococcus pneumoniae* pneumonia. Clin Microbiol Infec. **12**, 31-41

19 Maskell, J. P., Sefton, A. M. and Hall, L. M. C. (1997) Mechanism of sulfonamide resistance in clinical isolates of *Streptococcus pneumoniae*. Antimicrob. Agents Chemother. **41**, 2121-2126

20 Padayachee, T. and Klugman, K. P. (1999) Novel expansions of the gene encoding dihydropteroate synthase in trimethoprim-sulfamethoxazole-resistant *Streptococcus pneumoniae*. Antimicrob. Agents Chemother. **43**, 2225-2230

21 Vinnicombe, H. G. and Derrick, J. P. (1999) Dihydropteroate synthase: an old drug target revisited. Biochem. Soc. Trans. **27**, 53-58

22 Vinnicombe, H. G. and Derrick, J. P. (1999) Dihydropteroate synthase from *Streptococcus pneumoniae*: Characterization of substrate binding order and sulfonamide inhibition. Biochem. Biophys. Res. Commun. **258**, 752-757

23 Bermingham, A., Bottomley, J. R., Primrose, W. U. and Derrick, J. P. (2000) Equilibrium and kinetic studies of substrate binding to 6-hydroxymethyl-7,8-dihydropterin pyrophosphokinase from *Escherichia coli*. J. Biol. Chem. **275**, 17962-17967.

24 Sambrook, J., Fritsch, E. F. and Maniatis, T. (1989) Molecular Cloning: A Laboratory Manual. Cold Spring Harbor Laboratory Press, New York

25 Vanduyne, G. D., Standaert, R. F., Karplus, P. A., Schreiber, S. L. and Clardy, J. (1993) Atomic Structures of the Human Immunophilin Fkbp-12 Complexes with Fk506 and Rapamycin. J. Mol. Biol. **229**, 105-124

26 Pflugrath, J. W. (1999) The finer things in X-ray diffraction data collection. Acta Crystallogr. D. Biol. Crystallogr. **55**, 1718-1725

27 Terwilliger, T. C. and Berendzen, J. (1997) Bayesian correlated MAD phasing. Acta Crystallogr. D. Biol. Crystallogr. **53**, 571-579

28 Read, R. J. (2001) Pushing the boundaries of molecular replacement with maximum likelihood. Acta Crystallogr. D. Biol. Crystallogr. **57**, 1373-1382

29 Emsley, P. and Cowtan, K. (2004) Coot: model-building tools for molecular graphics. Acta Crystallogr. D. Biol. Crystallogr. **60**, 2126-2132

30 Murshudov, G. N., Vagin, A. A. and Dodson, E. J. (1997) Refinement of Macromolecular Structures by the Maximum Likelihood Method. Acta Crystallogr. D. Biol. Crystallogr. **53**, 240-255

31 CCP4. (1994) The CCP4 Suite:Programs for Protein Crystallography. Acta Crystallogr. D. Biol. Crystallogr. **50**, 760-763

32 Laskowski, R. A., McArthur, M. W., Moss, D. S. and Thornton, J. M. (1993) PROCHECK: a program to check the stereochemical quality of protein structures. J. Appl. Crystallogr. **24**, 946-950

33 Birdsall, B., King, R. W., Wheeler, M. R., Lewis, C. A., Goode, S. R., Dunlap, R. B. and Roberts, G. C. K. (1983) Correction for Light-Absorption in Fluorescence Studies of Protein-Ligand Interactions. Anal. Biochem. **132**, 353-361

34 Kuzmic, P. (1996) Program DYNAFIT for the analysis of enzyme kinetic data: Application to HIV proteinase. Anal. Biochem. **237**, 260-273

35 Lee, B. and Richards, F. M. (1971) The interpretation of protein structures: estimation of static accessibility. J. Mol. Biol. **55**, 379-400

36 Li, Y., Gong, Y. C., Shi, G. B., Blaszczyk, J., Ji, X. H. and Yan, H. G. (2002) Chemical transformation is not rate-limiting in the reaction catalyzed by *Escherichia coli* 6-hydroxymethyl-7,8-dihydropterin pyrophosphokinase. Biochemistry. **41**, 8777-8783

**Figure Legends**

**Figure 1 Reaction catalysed by DHPS.**

**Figure 2 Structure of *S. pneumoniae* DHPS and the binding of DHPP.** A) Ribbon plot of the *S. pneumoniae* DHPS dimer, with bound DHPP. One monomer is shown in magenta and the other in yellow. B) Fo-Fc electron density map, contoured at 2.5σ, superimposed on the DHPP ligand. C) Stereoview of the DHPP binding site. The side chains of selected residues, involved in DHPP recognition, are indicated. D) Detail showing the structural relationship between DHPP and Trp93 (magenta). Figures were created using PyMol (http://pymol.sourceforge.net/)

**Figure 3 Location of selected loop regions and comparison of the structures of *S. pneumoniae* and *S.aureus* DHPS.** A) Stereoview cartoon of *S. pneumoniae* DHPS monomer, showing the approximate locations of the loop regions with missing electron density (shown with dotted lines).. Loops 1, 2, and 5 and designated L1, L2 and L5 respectively. A spacefilling model of the DHPP ligand indicates the position of the active site. B) Stereoview cartoon comparison of the structures of *S. pneumoniae* DHPS (light grey) with *S. aureus* DHPS (dark grey). Figures were created using PyMol (http://pymol.sourceforge.net/)

**Figure 4 Equilibrium binding of PPi to sulfonamide sensitive *S. pneumoniae* DHPS measured from intrinsic protein fluorescence.** Enzymes used are as follows: sulfonamide sensitive DHPS (squares), Y63 (circles) and GS60 (triangles). Data points are means of 4 readings. The data were fitted to a single saturable binding site model with a $K_d$ of 350±20 μM and a fluorescence enhancement of 65%.

**Figure 5 Transient kinetics of the binding of PPi to sulfonamide sensitive *S. pneumoniae* DHPS recorded by stopped flow fluorimetry.** A) The sulphonamide sensitive form of *S. pneumoniae* DHPS (200 μg/ml), in one syringe, was rapidly mixed with PPi (600 μM) in the second syringe in a 1:1 volume ratio and the fluorescence recorded. The lower panel shows the difference between the recorded and predicted fluorescence values for a fitted exponential curve with an apparent rate constant ($k_{app}$) of 39$s^{-1}$. B) Variation in $k_{app}$ with [PPi]. Points are the means of duplicates. $k_{on}$ is 5.6±1.0 x $10^4$ $M^{-1}s^{-1}$ and $k_{off}$ is 21±3 $s^{-1}$. Other conditions are as for part A.

**Figure 6 Transient kinetics of DHPPP binding to sulfonamide sensitive *S. pneumoniae* DHPS recorded by stopped flow fluorimetry.** A) Sulfonamide sensitive form of DHPS (170 μg/ml), in one syringe, was rapidly mixed in a 1:1 volume ratio with DHPPP (100 μM) in the second syringe and fluorescence recorded. The results of four independent experiments were averaged. The lower panel shows the difference between the recorded and predicted fluorescence values for a fitted exponential curve with an apparent rate constant ($k_{app}$) of 22.6 $s^{-1}$. B) Variation in $k_{app}$ with [DHPPP]. Points are the means of duplicates. $k_{on}$ (gradient) is 2.6±0.2 x $10^5$ $M^{-1}s^{-1}$ and $k_{off}$ (intercept) is 8.7±1.3 $s^{-1}$. Other conditions are as for part A.

**Figure 7 Equilibrium fluorescence titrations to determine pABA binding affinity**

A) Titration of pABA into 500 μM PPi with varying concentrations of sulfonamide sensitive *S. pneumoniae* DHPS: squares, 50 μg/ml; diamonds, 100 μg/ml; triangles, 150 μg/ml. Data points are the

means of four separate measurements. The data were fitted to a compulsory order binding model, as outlined in the text. The $K_d$ for pABA was determined to be 0.13±0.02 μM. B) Titration of PPi into Y63 DHPS (150 μg/ml) in the presence of 40 μM (triangles) and 80 μM (squares) pABA. The $K_d$ for pABA was determined to be 50±6 μM.

**Table 1**

**X-Ray data processing and refinement statistics**

| Data Set | Selenomethionine | Native | DHPP Complex |
|---|---|---|---|
| X-ray source | ESRF ID29 | SRS 14.1 | lab |
| Wavelength (Å) | 0.934 | 1.488 | 1.54 |
| Spacegroup | $P2_1$ | $P2_12_12_1$ | $P2_12_12_1$ |
| Unit Cell Dimensions (Å) | 47.0 149.7 88.8 β=97.6° | 45.6 90.4 138.7 | 45.7 90.6 136.6 |
| Resolution range (Å) | 34.4 – 2.32 (2.4 – 2.32) | 55.0-1.8 (1.9 – 1.80) | 68.3 – 2.4 (2.49-2.4) |
| Total No. Reflections | 368945 | 204898 | 89381 |
| No. Unique Reflections | 100279 | 65291 | 19124 |
| Average Redundancy | 3.68 (1.82)[a] | 3.43 (2.89) | 4.57 (2.22) |
| % Completeness | 96.7 (80.2) | 99.0 (93.9) | 83.5 (41.8) |
| $R_{merge}$ (%)[b] | 0.073 (0.191) | 0.05 (0.21) | 0.062 (0.287) |
| Output <I/sigI> | 11.6 (3.4) | 12.7 (4.5) | 15.2 (3.2) |
| | | | |
| Refinement resolution range (Å) | - | 45.2-1.8 (1.85-1.80) | 20-2.4 (2.46-2.40) |
| Nonhydrogen atoms | | | |
| All | - | 4796 | 4456 |
| Water | - | 518 | 160 |
| | | | |
| $R_{cryst}$ (%) | - | 19.4 (27.7) | 21.6 (27.4) |
| $R_{free}$ (%) | - | 24.0 (35.7) | 29.7 (42.5) |
| | | | |
| RMSD from ideal values | - | | |
| Bond distance (Å) | - | 0.022 | 0.017 |
| Bond angle (degrees) | - | 1.67 | 1.67 |
| Estimated overall coodinate error (Å) [c] | | 0.098 | 0.271 |
| Ramachandran plot statistics (%)[d] (excl. Gly, Pro) | | | |
| Most favored regions | - | 95.2 | 93.3 |
| Additionally allowed regions | - | 4.8 | 6.2 |
| Generously allowed regions | - | 0.0 | 0.4 |
| Disallowed regions | - | 0.0 | 0.0 |

[a] Values in parentheses refer to the outer resolution data shell
[b] $R_{merge} = \Sigma_{hkl}\Sigma_{sym}|I-<I>|/\Sigma_{hkl}I$
[c] based on maximum likelihood from REFMAC5[30]
[d] from PROCHECK[32]

**Table 2**
**Rate and equilibrium constants for the binding of DHPPP to sulfonamide sensitive and resistant *S. pneumoniae* DHPS**

| | $k_{on}$ ($M^{-1}s^{-1}$) | $k_{off}$ ($s^{-1}$) | $K_d$ (μM)[a] |
|---|---|---|---|
| Sulfonamide sensitive | 2.6±0.2 x $10^5$ | 8.7±1.3 | 33±6 |
| Y63 | 2.4±0.1 x $10^5$ | 11±1 | 48±5 |
| GS60 | 2.6±0.2 x $10^5$ | 12±1 | 46±5 |

[a] Determined from $k_{on}$ and $k_{off}$ values.

Biochemical Journal Immediate Publication. Published on 05 Mar 2008 as manuscript BJ20071598

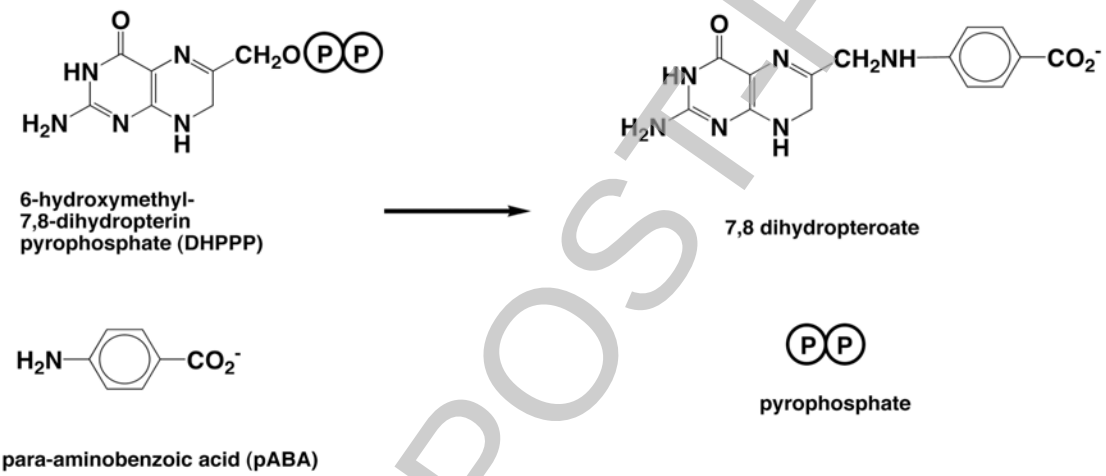


**Figure 1**

Biochemical Journal Immediate Publication. Published on 05 Mar 2008 as manuscript BJ20071598

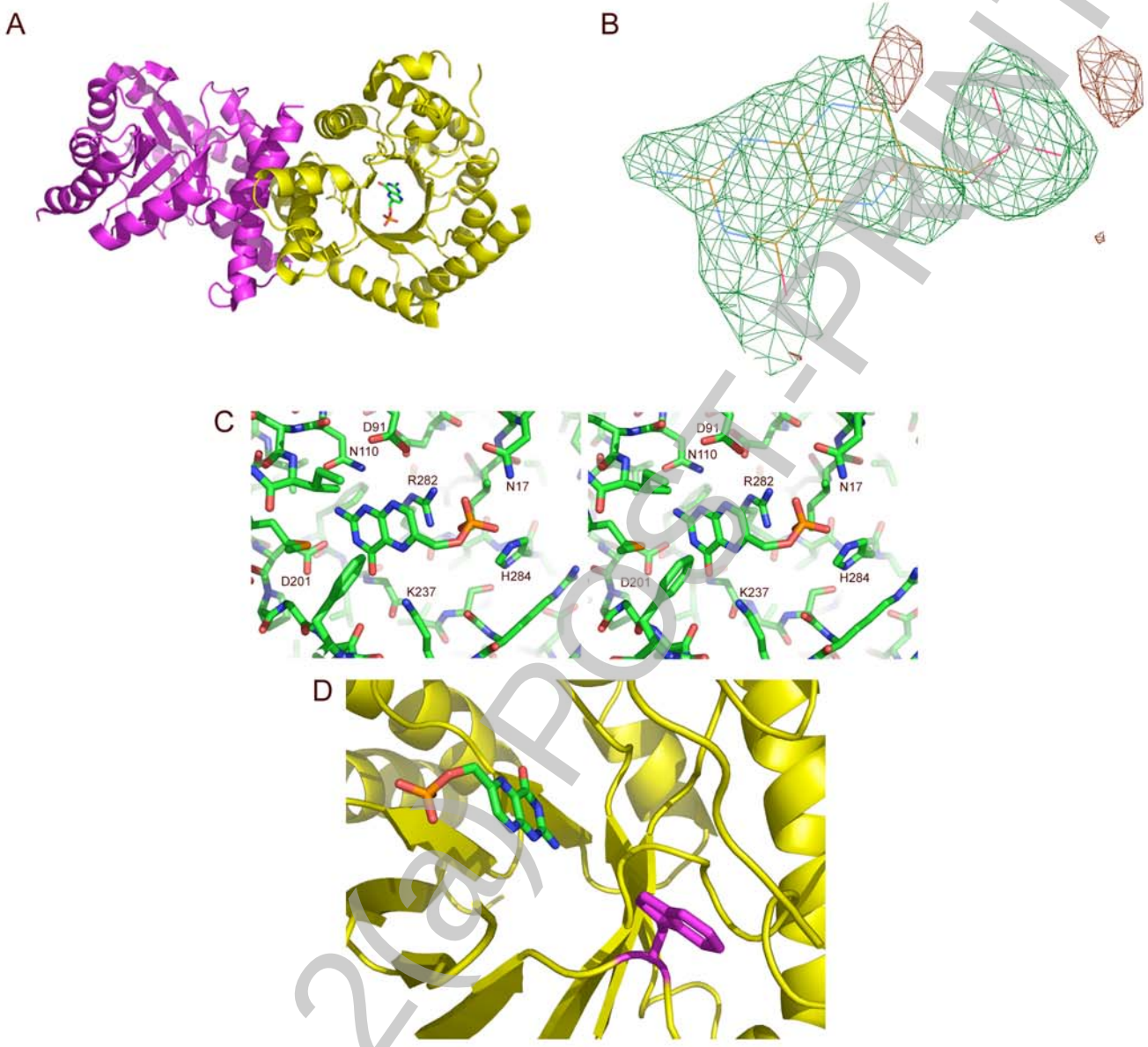


**Figure 2**

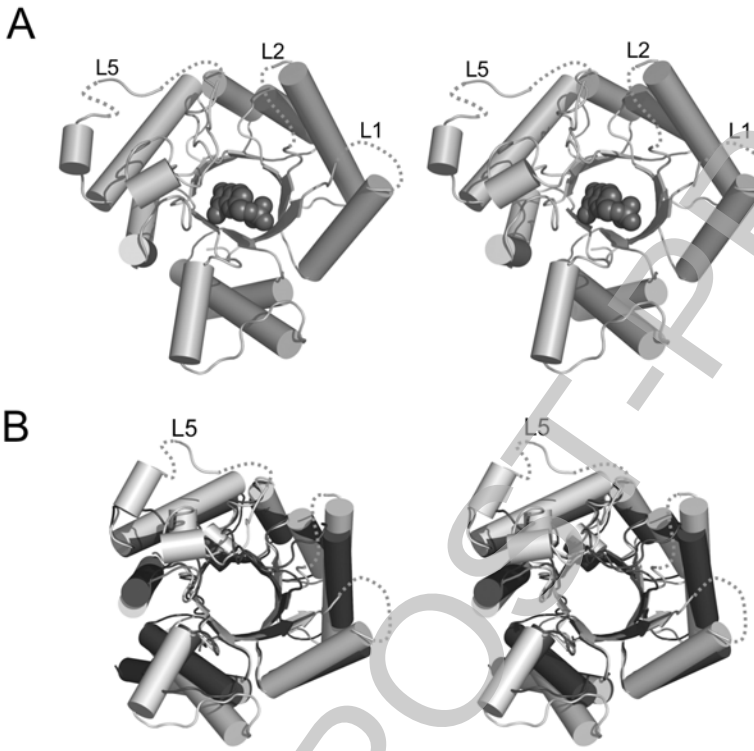


Figure 3

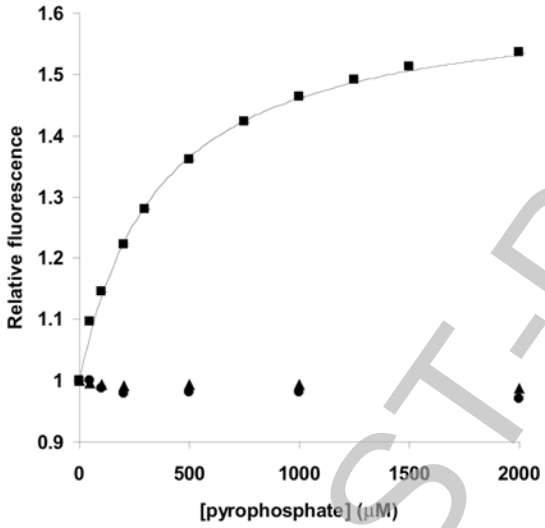


**Figure 4**

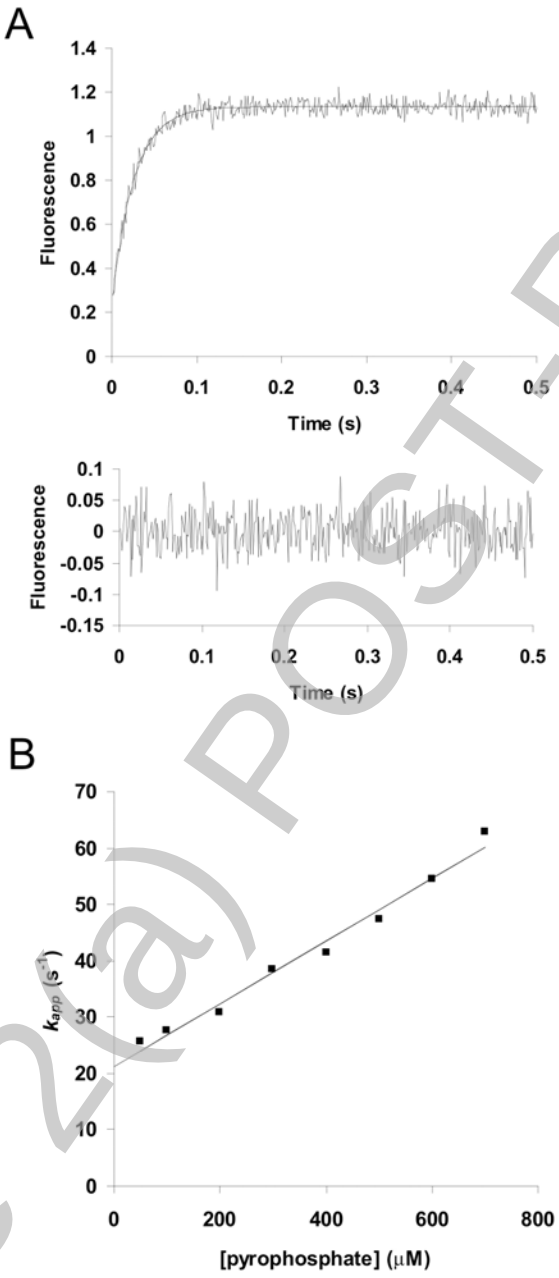


Figure 5

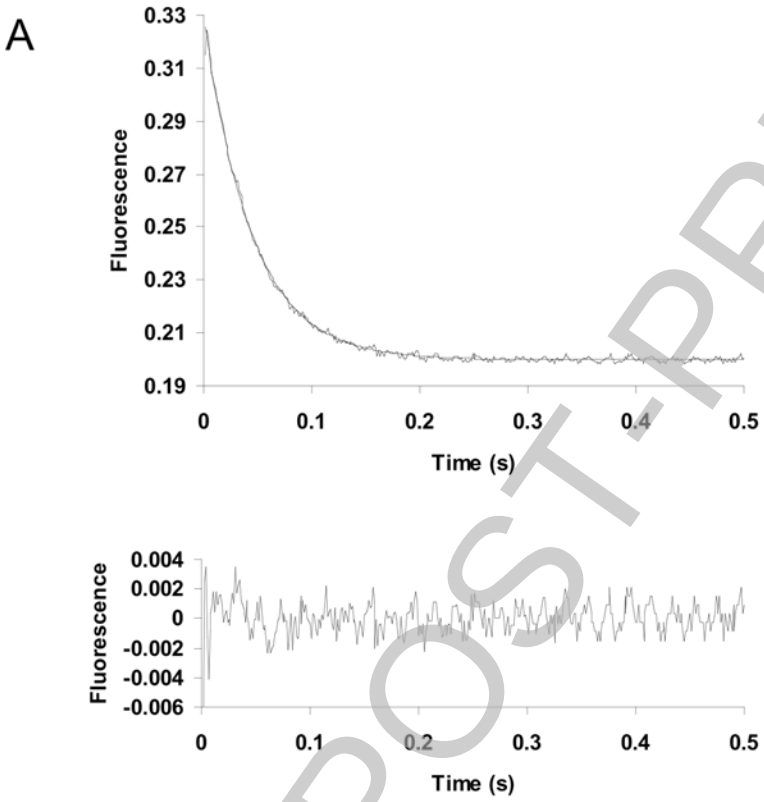


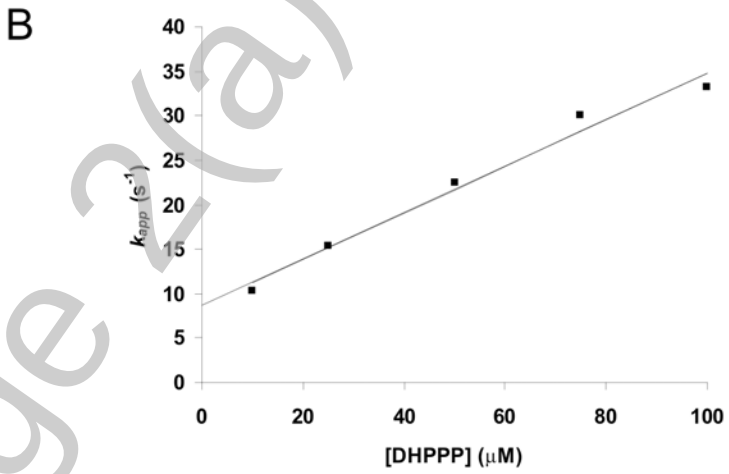


Figure 6

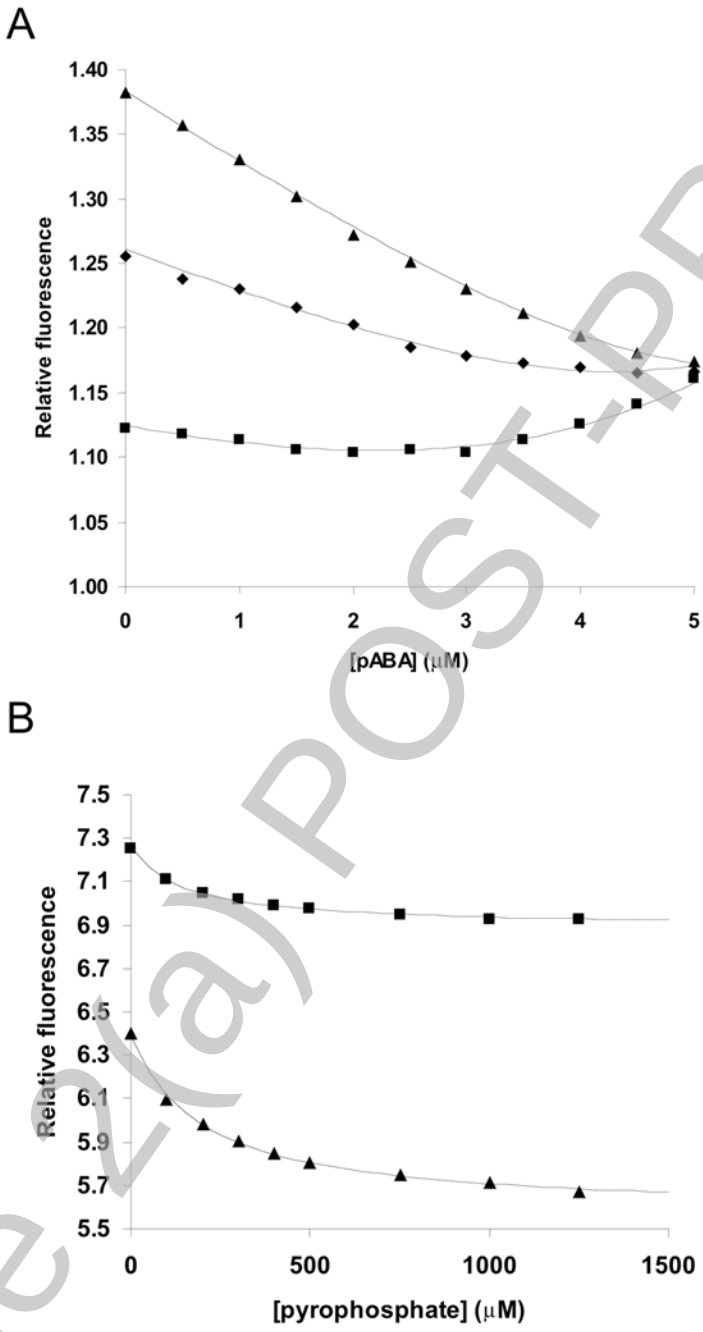


Figure 7